Detections of Multi-Periodic Oscillations during a Circular Ribbon Flare

Zongjun Ning[1,2] · **Ya Wang**[1] ·
Zhenxiang Hong[1,2] · **Dong Li**[1]

Abstract We present the analysis of three kinds of oscillating behavior using multi-wavelength observations of the 10 November 2013 (SOL2013-11-10T05:14) circular-ribbon flare. This event is a typical circular-ribbon flare with an outer spine structure and homologous jets. We found three kinds of oscillations (or perturbation): i) flux oscillation (or QPP) with a dominant period of about 20 seconds at X-rays, EUV and microwave emissions, ii) periodic jets with an intermittent cadence of around 72 seconds, iii) outer loop perturbs a half cycle with the duration of about 168 seconds. Similar to the periodic jets that could be produced by a nonthermal process, like repeated magnetic reconnection, the flare QPP detected in thermal emissions could have the same origin as the oscillation seen in nonthermal emissions. The outer loop perturbation is possibly triggered by a blast wave driven by the circular-ribbon flare, or it might be modulated by the sausage wave or the slow magnetoacoustic wave. The results obtained provide data for further numerical study of the physical origin of flare oscillations.

Keywords: Solar flares — Solar oscillations — Solar ultraviolet emission — Solar X-ray emission — Solar radio emission

1. Introduction

A solar flare is a powerful and impulsive process of magnetic-free-energy release in the solar atmosphere (see Benz, 2017, for a recent review). Solar-flare topology

✉ D. Li
lidong@pmo.ac.cn

Z. J Ning
ningzongjun@pmo.ac.cn

[1] Key Laboratory of Dark Matter and Space Astronomy, Purple Mountain Observatory, CAS, Nanjing 210023, China

[2] School of Astronomy and Space Science, University of Science and Technology of China, Hefei 230026, China

often shows elongated structures seen in the Hα, white light, and ultraviolet (UV) wavelengths, called "flare ribbons". Typically, two ribbons are located in regions of opposite magnetic polarities, which are parallel to the magnetic polarity inversion line (PIL) and separated the polarities. This is known as the " two-ribbon flare" (a detailed sketch can be seen in Priest and Forbes (2002)) and could be well explained by the classical 2D-reconnection model (Sturrock and Coppi, 1964; Shibata and Magara, 2011; Yan et al., 2018). However, a solar flare actually occurs in a more complicated structure associated with the 3D magnetic null point, i.e. the fan–spine topology (Török et al., 2009). The null point is mainly passed through by the inner and outer spine field lines, and the closed separatrix surface is dominated by the fan structure with a dome-like shape. The magnetic fields at the inner spine footpoint are opposite to those of the dome-shaped fan, producing a circular PIL. This erupted feature is called "circular-ribbon flare" (Masson et al., 2009; Wang and Liu, 2012), which is regarded as a result of the null-point reconnection. A schematic picture illustrating the main components and geometry structures of the circular-ribbon flare was provided by Wang and Liu (2012). During its eruption, the flare radiation at the footpoint of fan field lines is largely constituting a closed circular ribbon, and at the footpoints of inner spine field lines is a compact source called as central/inner ribbon. On the other hand, the outer spine field lines could be closed or open, and a remote/outer ribbon is formed at the footpoint of the closed outer spine field lines, while a series of homologous jets could be successively produced along the magnetic-field lines of the open outer spine (e.g. Chifor et al., 2008; Liu et al., 2011; Reid et al., 2012; Hao et al., 2017; Hernandez-Perez et al., 2017; Li et al., 2018b; Song and Tian, 2018; Zhang et al., 2021). This combination of factors results in various kinds of oscillations relating to this type of flare (Mészárosová et al., 2013; Kumar, Nakariakov, and Cho, 2015; Kashapova et al., 2020; Zhang, 2020).

Quasi-periodic pulsations (QPPs) are intensity oscillations during solar flares (e.g. Van Doorsselaere, Kupriyanova, and Yuan, 2016; McLaughlin et al., 2018; Zimovets et al., 2021). They often appear as a series of regular and periodic pulses in the flare light curve, which could be detected in a broad range of wavelengths, i.e. radio/microwave emissions (Ning et al., 2005; Kupriyanova et al., 2010; Nakariakov et al., 2018; Karlický and Yasnov, 2021), Hα (Srivastava et al., 2008; Yang and Xiang, 2016; Kashapova et al., 2020; Li et al., 2020b) and Lyα (Milligan et al., 2017; Li et al., 2020c; Li, 2021; Lu et al., 2021) emissions, UV or extreme-UV (EUV) wavelengths (Pugh et al., 2017; Shen et al., 2018; Kobanov and Chelpanov, 2019; Yuan et al., 2019), soft/hard X-ray (SXR/HXR) channels (Ning, 2014; Inglis et al., 2016; Li and Zhang, 2017; Kolotkov et al., 2018; Hayes et al., 2020), and even γ-ray emission (Nakariakov et al., 2010b; Li et al., 2020d). Such oscillatory features have also been observed in the circular-ribbon flare (Mészárosová et al., 2013; Kumar, Nakariakov, and Cho, 2015; Kashapova et al., 2020). A typical flare QPP is generally characterized by repeating and periodicity, and the quasi-periods can be observed from sub-seconds through seconds and minutes to dozens of minutes (Fleishman et al., 2002; Tan et al., 2010; Dolla et al., 2012; Kolotkov et al., 2015; Kupriyanova et al., 2016; Ning, 2017; Yu and Chen, 2019; Clarke et al., 2021; Li et al., 2021b). It seems that the

various periods of flare QPPs are always dependent on the detected wavelengths or the temporal resolution of the measuring instruments (see Kupriyanova et al., 2020, for a recent review). These properties indicate the possibility of generating flare QPPs with various periods by different mechanisms (e.g. McLaughlin et al., 2018; Kupriyanova et al., 2020). The short-periodicity QPPs (i.e. sub-seconds) are generally observed in radio or HXR emissions due to their high temporal resolution, which are most likely associated with the kinetic process driven by the dynamical interaction between electromagnetic plasmas and energetic particles trapped in the flaring loop (e.g. Aschwanden, 1987; Fleishman et al., 2002; Ning et al., 2005; Tan et al., 2010; Yu and Chen, 2019). The flare QPPs with long periods on the orders of seconds and minutes could be discovered in a broad wavelength range, such as microwave, white light, UV/EUV, SXR/HXR, and even γ-rays (Nakariakov et al., 2010b; Dolla et al., 2012; Kolotkov et al., 2015; Li and Zhang, 2017; Kobanov and Chelpanov, 2019; Li et al., 2020b; Hayes et al., 2020; Li, 2021). They are probably related with the magnetohydrodynamic (MHD) waves in complicated magnetic configurations at the flare region, or might be associated with the solar global oscillations (Ofman and Wang, 2002; Tian et al., 2016; Kupriyanova et al., 2016; Shen et al., 2018; Kolotkov et al., 2018; Yuan et al., 2019; Nakariakov and Kolotkov, 2020; Clarke et al., 2021).

Flare QPPs have attracted a lot of attention since they were first found in solar X-ray emissions (Parks and Winckler, 1969). However, the physical mechanism responsible for the generation of flare QPPs is still an open issue (Van Doorsselaere, Kupriyanova, and Yuan, 2016; McLaughlin et al., 2018; Kupriyanova et al., 2020). They are generally attributed to MHD waves in slow mode, kink mode, or sausage mode (Yuan and Van Doorsselaere, 2016; Li et al., 2020a; Nakariakov and Kolotkov, 2020; Nakariakov et al., 2021; Amiri, Karami, and Ebrahimi, 2021; Wang et al., 2021). They might also be caused by repetitive magnetic reconnection, which could accelerate nonthermal electrons and produce flare emission with quasi-periodic pulses (e.g. Kliem, Karlický, and Benz, 2000; Chen and Priest, 2006; Nakariakov and Zimovets, 2011; Kumar, Nakariakov, and Cho, 2015; Li and Zhang, 2015; Guidoni et al., 2016; Yuan et al., 2019; Li et al., 2020d). On the other hand, the flare QPPs are also interpreted as a self-oscillatory process such as magnetic dripping (Nakariakov et al., 2010a; Li et al., 2020c), or may be explained by the magnetic tuning-fork model (Takasao and Shibata, 2016) and the LRC-circuit model (Tan et al., 2016; Chen et al., 2019; Li et al., 2020b). The supra-arcade downflows were found to collide with post-flare loops at different instances, which could lead to the quasi-periodicity of flare radiation at wavelengths of UV/EUV and X-ray (Cai et al., 2019; Xue et al., 2020; Samanta et al., 2021). Moreover, the flare QPPs are thought to be related with the fundamental physical process of solar flares, i.e. magnetic reconnection, energy release, particle acceleration, and also MHD waves (e.g. Nakariakov and Zimovets, 2011). Therefore, they are useful for remotely diagnosing the key physical parameters in flare regions (Brosius and Daw, 2015; Dominique et al., 2018; Yuan et al., 2019).

Thanks to high-resolution imaging telescopes in EUV/SXR channels, the spatial motions of displacements have been found in hot coronal loops, and they are regarded as coronal-loop oscillations, which are often related to solar

flares (e.g. Nakariakov et al., 1999; Aschwanden et al., 2002). The coronal-loop oscillations are also seen as Doppler-shift oscillations using spectroscopic observations (Wang et al., 2002; Tian et al., 2016; Li et al., 2018a). Their displacement amplitudes are found to range from sub-megameter to dozens of megameters (Anfinogentov, Nakariakov, and Nisticò, 2015; Su et al., 2018; Goddard and Nisticò, 2020; Nakariakov et al., 2021), and their oscillatory periods are strongly dependent on the loop lengths. While the ratio of the decay time to the oscillatory period is systematically related with the displacement amplitudes (Goddard and Nakariakov, 2016). Fast magnetoacoustic waves, detected as wavelet tadpoles, have been found in the fan structure of a circular-ribbon flare (Mészárosová et al., 2013). Recently, transverse oscillations have been discovered in the outer loop of a circular-ribbon flare, which are explained as the kink mode of the MHD wave (Zhang et al., 2020; Dai et al., 2021), largely due to their incompressibility or weak compressibility (Yuan and Van Doorsselaere, 2016; Amiri, Karami, and Ebrahimi, 2021). Those circular-ribbon flares were also found to be accompanied by repeated and homologous coronal jets. On the other hand, the transverse oscillations detected in coronal loops can also be interpreted as sausage-mode waves in the plasma loops, and they are often caused by density perturbation on the coronal loops (Tian et al., 2016; Lim, Nakariakov, and Moon, 2018; Li et al., 2020a). However, the sausage oscillations excited by circular-ribbon flares are rarely reported at the outer coronal loop.

In this study, we investigated three kinds of oscillating behaviors using multi-wavelengths observations; they all related to a circular-ribbon flare on 10 November 2013. The article is organized as follows: Section 2 introduces the observations and instruments, Section 3 presents the data analysis and our main results, and Section 4 gives the conclusion and discussion.

2. Observations and Instruments

We studied the solar flare on 10 November 2013. It was an X1.1-class flare and occurred in the active region of NOAA 11890 (S11W28). The event started at about 05:09 UT, reached maximum at around 05:14 UT, and ended at roughly 05:22 UT. The flare was simultaneously observed in multiple wavelengths, which was measured by the *Geostationary Operational Environmental Satellite* (GOES), the *Reuven Ramaty High Energy Solar Spectroscopic Imager* (RHESSI: Lin et al., 2002), the *Nobeyama RadioPolarimeters* (NoRP: Nakajima et al., 1985), the *Nobeyama RadioHeliograph* (NoRH: Hanaoka et al., 1994), *Konus-Wind* (Aptekar et al., 1995; Pal'shin et al., 2014), the *Gamma Ray Burst Monitor* (GBM) on *Fermi* (Meegan et al., 2009), the *Atmospheric Imaging Assembly* (AIA: Lemen et al., 2012), the *Helioseismic and Magnetic Imager* (HMI: Schou et al., 2012), and the *Extreme Ultraviolet Variability Experiment* (EVE: Woods et al., 2012) onboard the *Solar Dynamics Observatory* (SDO: Pesnell, Thompson, and Chamberlin, 2012); see the details in Table 1.

The X1.1 flare shows a closed circular ribbon and a faint remote ribbon, as well as a faint outer loop that connected the closed circular ribbon and a remote brightening, which is seen in 171 Å and 1600 Å images measured by SDO/AIA

Table 1. Instruments used to detect flare oscillations in this study.

Instruments	Cadence	Channels	Description	Observation
GOES/XRS	≈ 2 seconds	$1 - 8\,\text{Å}$	SXR	
		$0.5 - 4\,\text{Å}$	SXR	1D
RHESSI	4 seconds	$3 - 6\,\text{keV}$	SXR	
		$50 - 100\,\text{keV}$	HXR	2D
Fermi/GBM	≈ 0.256 second	$4.2 - 11.5\,\text{keV}$	SXR	
		$11.5 - 26.6\,\text{keV}$	SXR/HXR	1D
		$26.6 - 50.4\,\text{keV}$	HXR	
		$50.4 - 102.4\,\text{keV}$	HXR	
Konus-Wind	≈ 1.024 seconds	$20 - 80\,\text{keV}$	SXR/HXR	
		$80 - 300\,\text{keV}$	HXR	1D
		$300 - 1200\,\text{keV}$	HXR/γ-ray	
NoRP	0.1 second	1 GHz	Microwave	
		2 GHz	Microwave	
		3.75 GHz	Microwave	1D
		9 GHz	Microwave	
		17 GHz	Microwave	
		35 GHz	Microwave	
NoRH	1 second	17 GHz	Microwave	
		34 GHz	Microwave	2D
SDO/EVE	0.25 second	$0.1 - 7.0\,\text{nm}$	SXR	
		$17.2 - 20.6\,\text{nm}$	EUV	1D
		$23.1 - 27.6\,\text{nm}$	EUV	
		$28.0 - 32.6\,\text{nm}$	EUV	
SDO/AIA	12 seconds	$171\,\text{Å}$	EUV	
	24 seconds	$1600\,\text{Å}$	UV	2D
SDO/HMI	45 seconds	magnetogram	LOS	2D

shown in Figure 1a, b, and d, and the Electronic Supplementary Material movie. The AIA $1600\,\text{Å}$ image was obtained at 05:14:16 UT, which is around the flare maximum, while the AIA $171\,\text{Å}$ band image was taken at 05:15:59 UT. At this moment, the outer loop can be more clearly distinguished, especially in the running difference. The lines marked S1 − S3 show the positions of the slits on the outer loop. They are selected to study the jets and loop perturbation analyzing in the next section, and the red "$*$" symbols mark the zero of the y-axis in Figure 8. Figure 1c gives the line-of-sight(LOS) magnetogram obtained by SDO/HMI (Schou et al., 2012). A closed circular ribbon is associated with the negative magnetic polarity and an inner ribbon is on the compact positive magnetic polarity, while the faint remote ribbon is along the diffuse positive magnetic polarity. The flare event was also observed by the RHESSI and NoRH
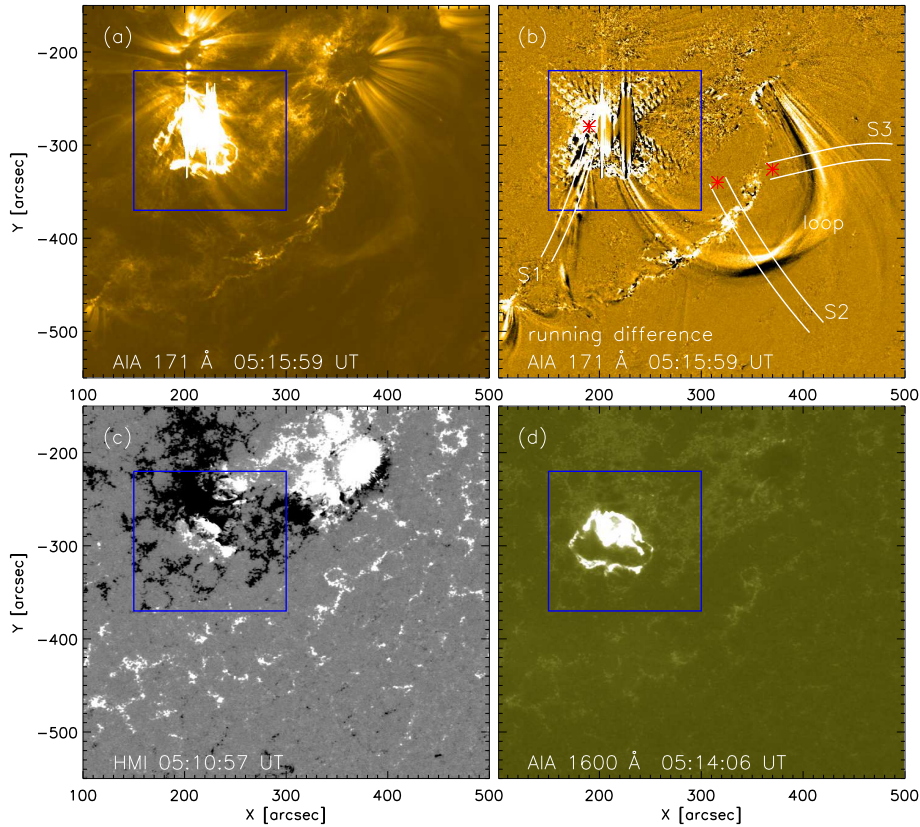
Figure 1. Panels **a** and **b**: AIA 171 Å and its running-difference images show the circular-ribbon flare with a FOV of $400'' \times 400''$. Three groups of solid lines outline the slit positions in Figure 8, and the *red symbols* of "*" indicate the zero of the *y*-axis. Panels **c** and **d**: HMI LOS magnetogram and AIA 1600 Å image with a FOV of $400'' \times 400''$. The *blue box* outlines a small FOV of about $150'' \times 150''$ shown in Figure 2**a** and **b**.

images in X-rays and microwaves, as indicated by the color contours in Figure 2a and b. The SXR and HXR images at $3-6\,\mathrm{keV}$ and $50-100\,\mathrm{keV}$ were reconstructed using the CLEAN algorithm from the RHESSI data for the time interval of one minute. This exposition allows improving the signal to noise ratio. Similar to the AIA 1600 Å band image, the microwave images are obtained at 05:14:16 UT. This event at the SXR $3-6\,\mathrm{keV}$ (blue contours) and microwave $17\,\mathrm{GHz}$ (green contours) and $34\,\mathrm{GHz}$ (cyan contours) shows one source, but double HXR footpoint sources at $50-100\,\mathrm{keV}$ (red contours), respectively. Both the SXR/HXR and microwave emissions appear to overlay the inner flare ribbon seen in the AIA 1600 Å band image. This is consistent with the standard flare model (e.g. Sturrock and Coppi, 1964; Shibata and Magara, 2011), for instance, the double footpoint sources of HXR at $50-100\,\mathrm{keV}$ (red contours) are located at the regions with different polarity magnetic fields: one is on the inner ribbon with negative polarity field; while another is on the circular ribbon with positive polarity.

The X-ray observations have different temporal resolutions from the other instruments (see Table1). It should be pointed out that the X-ray light curves recorded by *Konus-Wind* and *Fermi*/GBM are interpolated onto the uniform temporal resolution, i.e. 1.024 seconds for the *Konus-Wind* data (e.g. Li et al., 2020d) and 0.256 second for the *Fermi*/GBM data (see also, Li, Ning, and Zhang, 2015; Ning, 2017). The NoRP is a ground-based telescope, which provides solar microwave fluxes at six frequencies with a temporal cadence of ≈0.1 second (Nakajima et al., 1985). The *EUV SpectroPhotometer* for SDO/EVE measures the Sun at one SXR and three EUV wavebands with a time resolution of 0.25 second (Didkovsky et al., 2012; Woods et al., 2012). Similar to the GOES $1 - 8$ Å light curve, the ESP $0.1 - 7$ nm is a SXR flux. The ESP $17.2 - 20.6$ nm flux includes the line emission mostly from the coronal plasma at about $1 - 2$ MK, while the ESP $23.1 - 27.6$ nm and $28.0 - 32.6$ nm fluxes are mainly dominated by the He II line in the chromosphere (Didkovsky et al., 2012; Dolla et al., 2012; Li et al., 2021a).

3. Data Analysis and Results

3.1. NLFFF Extrapolation

To reveal the magnetic topology of the circular-ribbon flare region, we carried out nonlinear force-free field (NLFFF) extrapolation by using the optimization approach proposed by Wheatland, Sturrock, and Roumeliotis (2000) and further developed by Wiegelmann (2004). We used the HMI vector magnetogram retrieved from the HMI.B_720 seconds data series at about 05:00:00 UT as the bottom boundary. The 180-degree ambiguity in the transverse components of the vector magnetic field is removed by using the improved minimum energy method (Metcalf et al., 2006; Leka et al., 2009), and the projection effect was also corrected. Then, the vector magnetic field can be used as the boundary conditions after a preprocessing to satisfy the force-free and torque-free conditions on the photosphere (Guo, Cheng, and Ding, 2017). The extrapolation cube size is $232 \times 196 \times 196$ Mm^3. As shown in Figure 2c and d, the flare shows a spine–fan magnetic topology, which is similar to the previous result about the circular ribbon flare (e.g. Mészárosová et al., 2013). During the flare event, the dome-like structure is consistent with the closed circular ribbon that is accompanied by the occurrence of a series of coronal jets. It is also followed by the remote ribbon at the western end of the outer spine. In addition, a set of overlying magnetic field lines indicated by white lines matches well with the faint outer loop observed in AIA 171 Å. Consistent with the previous observation (e.g. Wang and Liu, 2012), this circular-ribbon flare has two HXR footpoint sources on the optic inner and circular ribbons, respectively. The microwave sources at 17 GHz (green contours) and 34 GHz (cyan contours) are between two HXR footpoint sources. It is reasonable that the microwave emissions at 17/34 GHz are produced by the electrons trapped in the flare loops (part of the fan structure in Figure 2c and d) though synchrotron radiation. The microwave source at 34 GHz is smaller than that at 17 GHz, due to it is from the higher electrons located near the footpoint
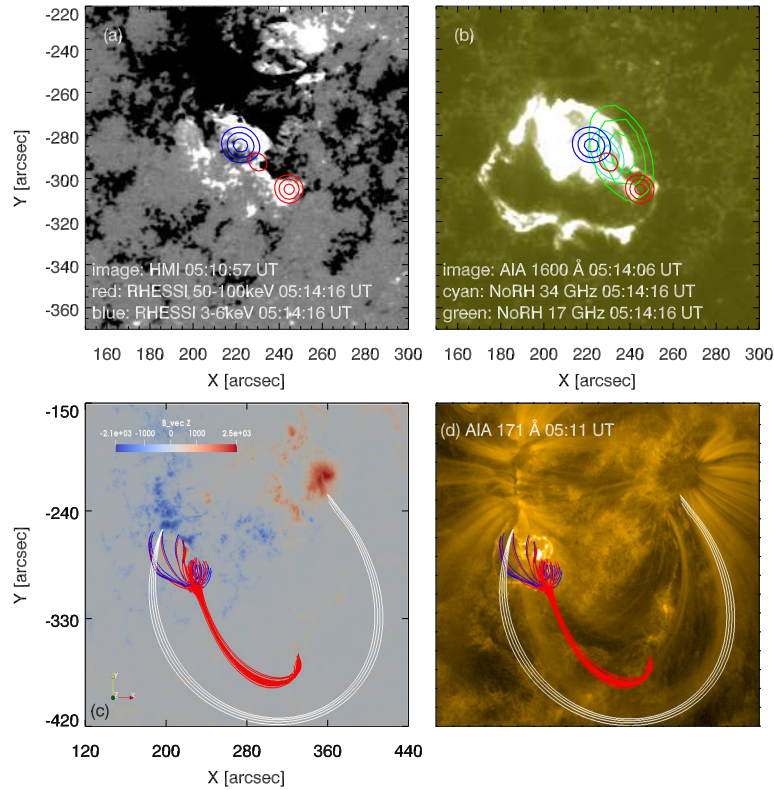
Figure 2. Panels **a** and **b**: HMI LOS magnetogram and AIA 1600 Å image with a small FOV. The *red and blue contours* represent the RHESSI X-ray emissions at $50-100$ keV and $3-6$ keV, while the *cyan and green contours* show the microwave emissions in NORH 34 GHz and 17 GHz. The levels are set at 50 %, 70 %, and 90 % of the maximum brightness of each detected channel. Panel **c**: Magnetic topology for the flare region in the $x-y$ plane observed from the z-direction. The Bz component on the bottom boundary ranges from -2.1×10^3 to 2.5×10^3 Gauss. Panel **d**: AIA 171 Å image at ≈05:11 UT overlaid with the extrapolated magnetic field lines. The *red and blue lines* represent the spine–fan magnetic topology, while the *white lines* indicate the overlying magnetic loop.

of magnetic loop. The thermal source of SXR at $3-6$ keV (blue contours) is not between two HXR footpoint sources, just on the top of the inner ribbon. Except for the projection effect, another possible location seems near the null point of the magnetic field, as shown in Figure 2 c and d. The null point is thought to be the reconnection site of the circular ribbon flare, and it is near the fan-structure top (the loop apex in the standard flare model) where the SXRs radiate.

3.2. Flux Oscillation During the Circular Ribbon Flare

To investigate the periodicity of this circular-ribbon flare, we first perform the Fast Fourier Transform (FFT) for the raw light curves in SXR $1-8$ Å (black) and $0.5-4$ Å (magenta) measured by the GOES, as shown in Figure 3. Similar to previous results (e.g. Inglis et al., 2016; Kolotkov et al., 2018; Hayes et al., 2020; Li et al., 2020d; Wang et al., 2020), each Fourier power spectrum of the raw light curve shows two dominant features – a power-law spectrum and a flat spectrum, as indicated by the green lines in Figure 3. The first one often relates to red noise, while the other spectrum is usually considered as white noise in solar physics and astrophysics (e.g. Vaughan, 2005; Liang et al., 2020; Anfinogentov et al., 2021). The FFT power spectra show a clear peak above the 99% significance level (cyan lines) at a value that is close to about 20 seconds, as indicated by the vertical dotted lines. We would like to note that the FFT peaks are a bit broad, and they do not appear above 30 seconds, as shown by the vertical dashed line. On the other hand, the FFT spectrum at GOES $0.5-4$ Å demonstrates double peaks close to 40 seconds, which are absent in the GOES $1-8$ Å flux. Therefore, only the period of about 20 seconds for the flare flux is considered in the current study.

Figure 4 presents the analysis of periodicity for the circular-ribbon flare recorded by the GOES. Similar to a typical solar flare, this event exhibits an impulsive increasing and a slow decay phase, and no obvious QPP signature is seen in the raw SXR light curves. This is because the flare QPPs in the GOES SXR flux often show a very small amplitude superimposed on a strong background emission (e.g. Simões, Hudson, and Fletcher, 2015; Feng et al., 2017, 2020; Kolotkov et al., 2018; Hayes et al., 2020). Therefore, the strong background emission should be removed from the original data. In this study, the raw light curve is first decomposed into a slowly varying component and a rapidly varying component using the FFT (Ning, 2014, 2017; Li and Zhang, 2017; Milligan et al., 2017). Figure 3 suggests that the flare QPP in the GOES $1-8$ Å and $0.5-4$ Å shows a clear period near 20 seconds, so a cutoff threshold of 30 seconds is applied, as marked by the vertical dashed line in Figure 3. Thus, the long-term trend is suppressed, while the short period can be highlighted in the wavelet power spectrum (Kupriyanova et al., 2010; Kolotkov et al., 2015; Kashapova et al., 2020). Here, the slowly varying components are multiplied by 0.9 to avoid overlapping with the raw light curves, as shown by the blue curves in Figure 4a. The rapidly varying components during the flare are presented in Panel b, as outlined by two vertical dashed lines in Figure 4a. They are characterized by a series of pulses. Then, the wavelet-analysis method (Torrence and Compo, 1998) is applied to the rapidly varying component seen in GOES $1-8$ Å, as shown in Panel c. The wavelet power spectrum confirms a broad range of enhanced power that is centered at about 20 seconds, suggesting a dominant period of about 20 seconds. However, the enhanced power focuses on the impulsive phase in the GOES SXR channel, largely due to the fact that the amplitudes of flare QPPs are changed with time. Figure 4b shows some pulses with a small amplitude during the flare decay phase. In order to rule out the noise, we set a threshold ($\pm 3\sigma$) to identify the flare QPP pulses. Here, σ represents the standard deviation
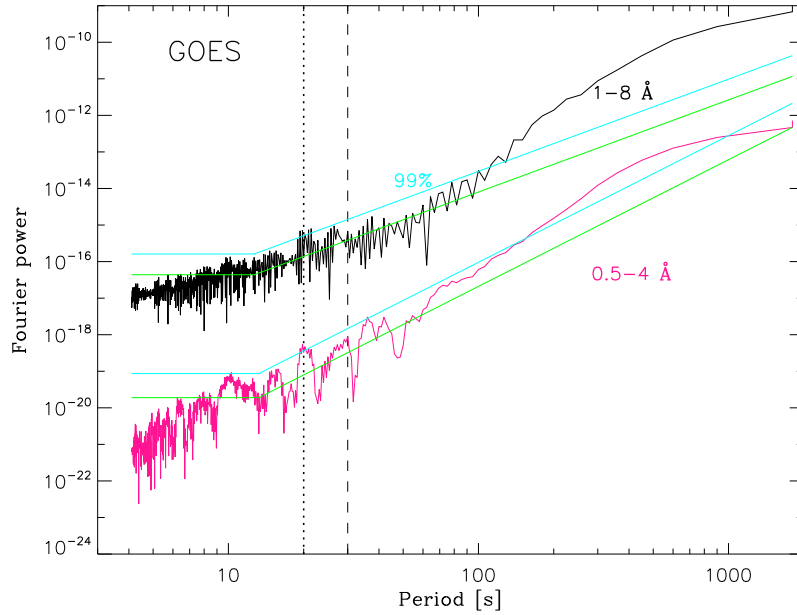
Figure 3. Fourier power of the flare light curves measured by the GOES at $1-8$ Å (*black*) and $0.5-4$ Å (*magenta*). The vertical dotted and dashed lines mark the positions at the periodicity of 20 seconds and 30 seconds. The *green lines* are the best fit, and the *cyan lines* represent the 99 % significance level.

of the rapidly varying component. Only these pulse amplitudes that are greater than the threshold are regarded as valid pulses, as shown by the blue-dashed lines in Panel b. Then, each valid pulse of the rapidly varying component at the GOES $1-8$ Å is normalized by its pulse amplitude, as shown in Panel d. Finally, Panel e displays the wavelet power spectrum for the normalized rapidly varying component, which exhibits a dominant period of roughly 20 seconds during the flare time. i.e. from the impulsive phase to the decay phase. This is consistent with the 20-second period in the FFT power spectra in Figure 3.

In addition to GOES, the X1.1 flare was also observed by NoRP, RHESSI, *Konus-Wind*, SDO/EVE, and *Fermi*/GBM in radio/microwave, X-ray, and EUV, as shown in Table 1. Similar to the GOES full-disk flux, any of them detect the solar radiation from the entire Sun. We should point out that RHESSI provided imaging spectroscopy, but we focused on the whole disk (Sun-as-a-star) observations in this study. The RHESSI light curve is not used for periodicity testing here, because there were several changes of attenuators (see, hessi.ssl.berkeley.edu/hessidata/metadata/2013/11/10/hsi_20131110_040600_rate.png). Then, the same wavelet-analysis method (Torrence and Compo, 1998) is used for the periodicity testing in the microwave, SXR/HXR, and EUV wavelengths; the detailed results can be seen in Figures $5-7$. The raw light curves (black) are decomposed into slowly (blue) and rapidly varying components, as shown in Panels a1, a2, b1, and b2 in Figures 5 and 6. The slowly varying components are multiplied by 0.9 to avoid overlapping with the raw light curves, and some
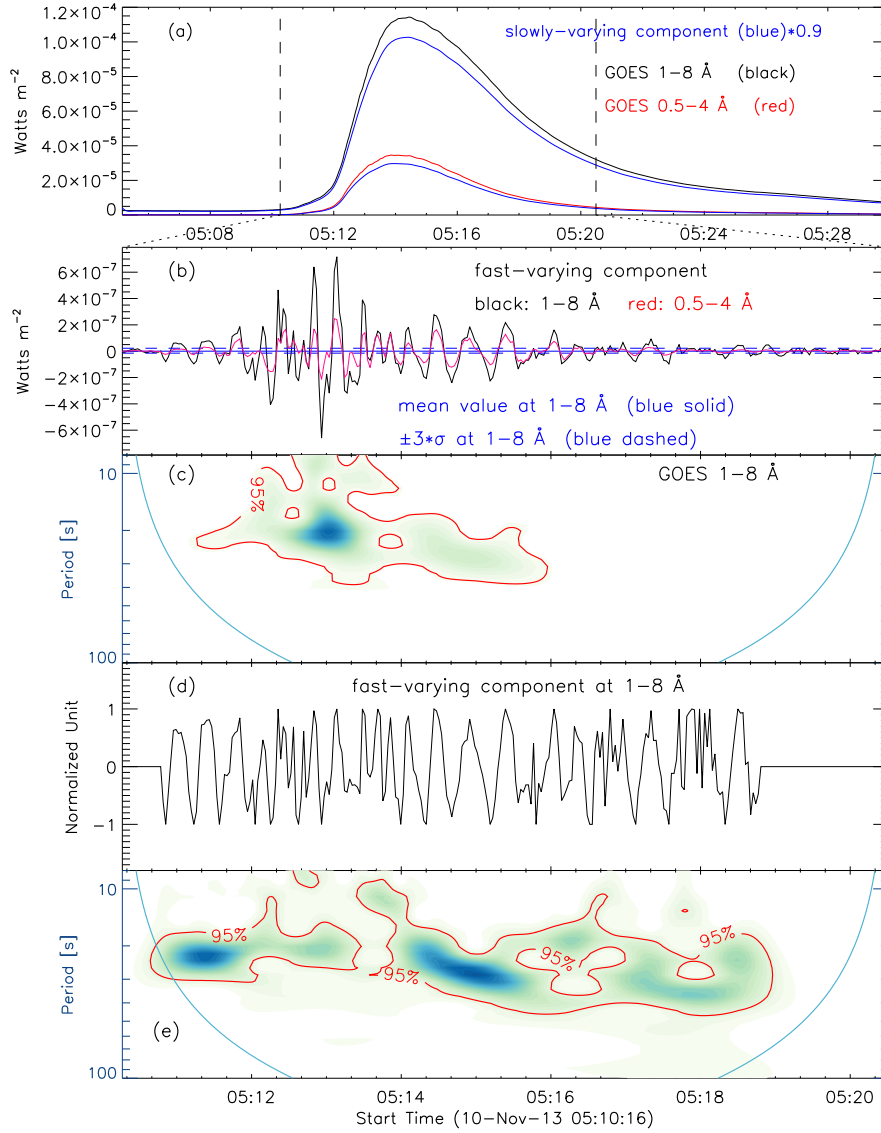
Figure 4. Panel **a**: SXR light curves in GOES $1-8\,\text{Å}$ (*black*), and $0.5-4\,\text{Å}$ (*red*) for the 10 November 2013 solar flare, and their slowly varying component (*blue*, after multiplying by 0.9. Panels **b** and **c**: Rapidly varying components of GOES SXR fluxes in the time interval between the two vertical dashed lines in Panel **a** and its wavelet power spectrum. The blue solid and dashed lines represent the mean and $\pm 3\sigma$ at GOES $1-8\,\text{Å}$. Panels **d** and **e**: the normalized rapidly varying component at GOES $1-8\,\text{Å}$ and its wavelet power spectrum. The *red contours* represent a significance level of 95 %. Anything 'outside' the *light blue curve* in Panels **c** and **e** is dubious.
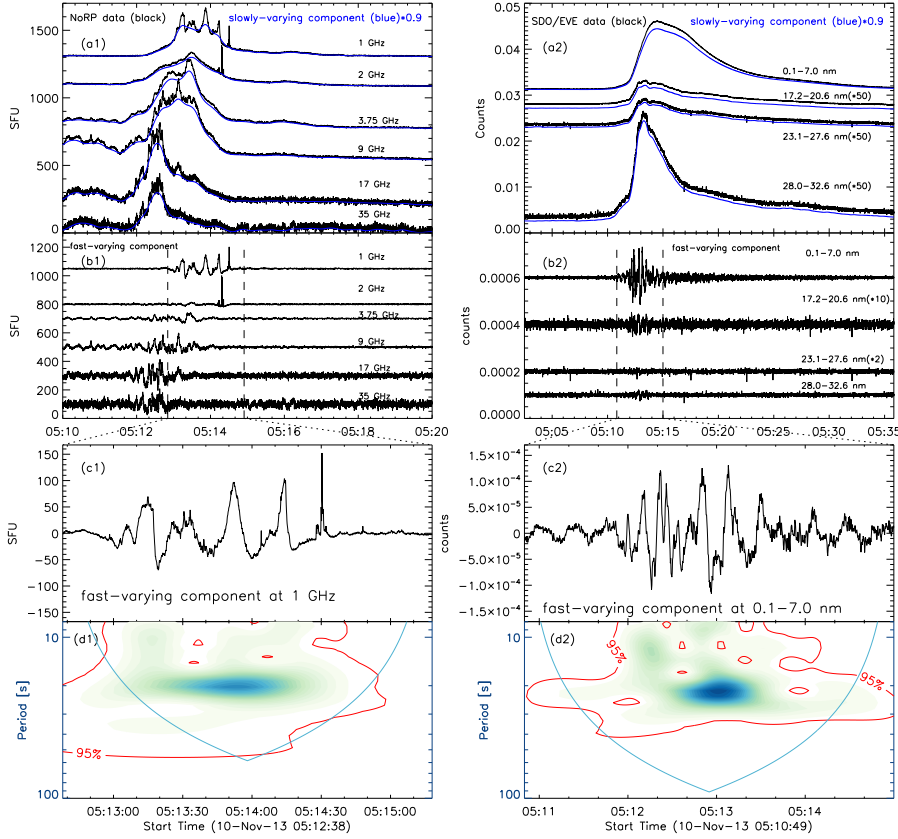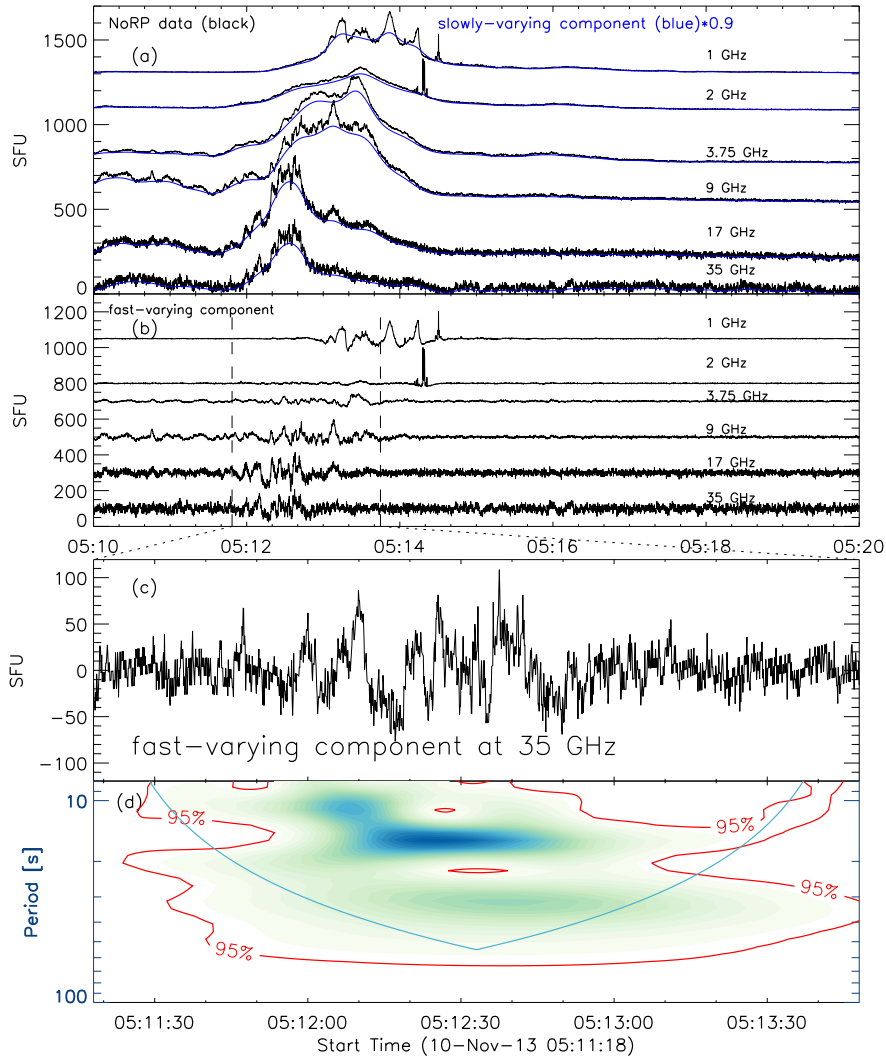
Figure 5. Similar to Figure 4, the light curves (*black*) detected by the NoRP, and the SDO/EVE, and their slowly varying components (*blue*, after multiplying by 0.9), as well as the rapidly varying components in time intervals between the two vertical dashed lines and their wavelet power spectra at NoRP 1 GHz, SDO/EVE 0.1 – 7 nm, respectively. The *red contours* represent a significance level of 95 %.

light curves have been shifted in height, so that they can be displayed clearly in the same window. Panels c1 and c2 present the rapidly varying components at channels of NoRP 1 GHz, ESP 0.1 – 7 nm, KW 20 – 80 keV, and Fermi 26.6 – 50.4 keV during the flare, as indicated by two vertical dashed lines in Panels b1 and b2. Here, the NoRP flux at the frequency of 1 GHz is used to perform the wavelet analysis, because it exhibits the most obvious oscillation, as shown in Figure 5a1 and b1. ESP 0.1 – 7 nm on SDO/EVE is applied to perform the wavelet analysis, as it is very similar to the GOES SXR flux. The other light curves measured by NoRP and SDO/EVE also show the QPP feature, but they are very weak, in particular for the EUV flux at ESP 28.0 – 32.6 nm, as shown in Figure 5b1. Therefore, the wavelet power spectra in the NoRP 1 GHz, ESP 0.1 – 7 nm, KW 20 – 80 keV, and Fermi 26.6 – 50.4 keV are presented here, which show that the pulsation is strongest at the periodicity of 20 seconds, but
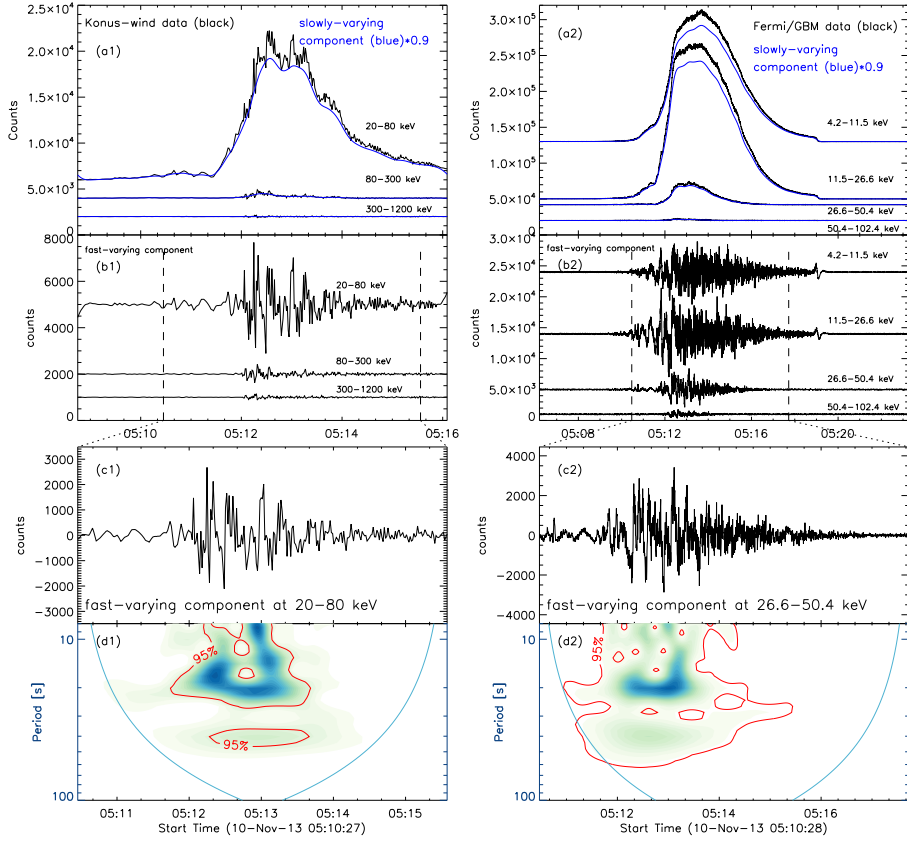
Figure 6. Similar to Figure 4, the light curves (*black*) detected by the *Konus-Wind*, and the *Fermi*/GBM, and their slowly varying components (*blue*, after multiplying by 0.9), as well as the rapidly varying components in time intervals between the two vertical dashed lines and their wavelet power spectra at KW $20-80$ keV, and *Fermi* $26.6-50.4$ keV, respectively. The *red contours* represent a significance level of 95 %.

the oscillation period is not exactly 20 seconds. It is spread over a broad range of periods, but centered at about 20 seconds. This is similar to the previous finding obtained from the GOES SXR flux. Physically, the microwave emission indicates nonthermal processes at frequencies above the frequency related to the flux maximum, the so-called "peak frequency". In the current case, the microwave emission at NoRP 35 GHz is exactly above the "peak frequency". Thus, we also present the wavelet analysis method for the microwave flux at the frequency of NoRP 35 GHz, as shown in Figure 7. Similar to previous results, the wavelet power spectrum shows an enhanced power over a broad range of periods, and the strongest power is centered at about 20 seconds. On the other hand, the onset time of the 20-second QPP in NoRP 35 GHz is earlier than that in NoRP 1 GHz, i.e. one minute earlier.

Figure 7. Similar to Figure 4, the light curves (*black*) detected by the NoRP, and their slowly varying components (*blue*, after multiplying by 0.9), as well as the rapidly varying components in time intervals between the two vertical dashed lines and their wavelet power spectra at NoRP 35 GHz. The *red contours* represent a significance level of 95 %.
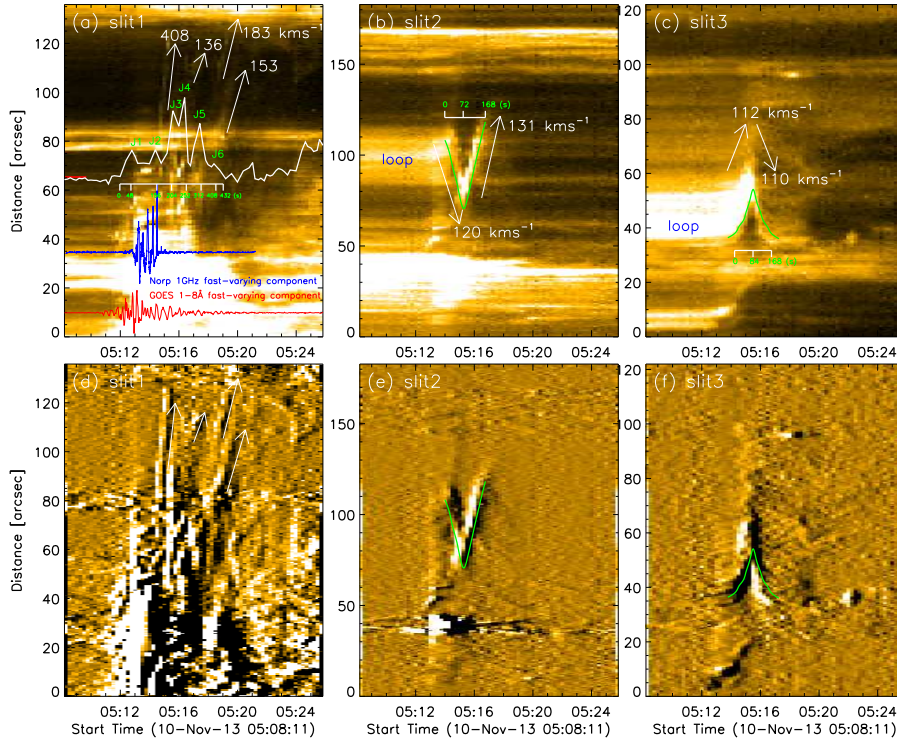
3.3. Periodic Jets Triggered by the Circular Ribbon Flare

Figure 8 shows the time–distance images along three slits derived in AIA 171 Å image series (a–c) and their running-difference images (d–f). As shown in Figure 1, a faint outer loop appears in AIA 171 Å during the X1.1 flare, and it connects the closed circular ribbon and the remote brightening. Here, the slits are selected to cross the footpoint (S1), the loop apex (S2), and the loop leg (S3)

for the outer loop, as outlined by the white curves in Figure 1b. Panels a and d plot the time–distance images along the Slit 1 (S1) at the footpoint, the bright emission at the bottom is emitted from the closed circular ribbon of the X1.1 flare, which is accompanied by a series of coronal jets. The coronal jets are very weak in the original image, but they are much clearer in the running-difference image, which are characterized by the dark oblique stripes, as indicated by the white arrows in Panel d. The coronal jets exhibit a fast speed that could reach to be about $408\,\mathrm{km\,s^{-1}}$. The average jet velocity is estimated by the slope of dark oblique stripes in the running-difference image. The jets periodically occurred. We plotted the intensity variations (white) along the $66''$ marked by the red line on Panel a. The intensity curves show six peaks corresponding to six jets as $J1-J6$ marked on timescale during the time interval of $\approx 432\,\mathrm{seconds}$. Thus, the average cadence of coronal jets is about $72\,\mathrm{seconds}$. However, we could not find the similar quasi-period in the X-ray or microwave flux. The overplotted blue and red lines are the rapidly varying components in NoRP $1\,\mathrm{secondsGHz}$ and GOES $1-8\,\mathrm{\AA}$ in Figure 8a. They both show the short-period oscillation, i.e. a dominant period of $20\,\mathrm{seconds}$, which is much shorter than the average cadence of coronal jets. Moreover, the 20-second oscillation at GOES and NoRP occurs at the same interval between about 05:12 UT and 05:15 UT as the first two jets of J1 and J2, while the other jets from J3 to J6 appear at the time after 05:16 UT when the 20-second oscillation disappears.

3.4. Transverse Perturbation of the Outer Loop

Figure 8b and c present the time–distance images along the slits S2 and S3: the zero of the y-axis is marked by the red "*" in Figure 1b. The outer loop shows the transverse perturbation consisted of a half cycle only, for instance, it displaces from the equilibrium position, reaches maximum displacement, and returns back to the equilibrium without overshooting. The transverse perturbation has a duration of about $168\,\mathrm{seconds}$. The onset of perturbation coincided with the flare eruption, see also the movie in AIA $171\,\mathrm{\AA}$ channel. The perturbation amplitude is very large, maybe as high as $20\,\mathrm{Mm}$, suggesting a large-amplitude perturbation. It is interesting that the loop apex (S2) shows an anti-phase perturbation with the loop leg (S3). In other words, the loop apex is shrinking, while the loop leg is expanding. Figure 8e and f give their time–distance images after running-difference. Figure 9 shows the running-difference images in the AIA $171\,\mathrm{\AA}$ band. The temporal cadence to perform the running difference image is $24\,\mathrm{seconds}$ rather than $12\,\mathrm{seconds}$. This is because that the AIA images have two different exposure times during this solar flare. Consistent with the anti-phase perturbations in Figure 8e and f, the different parts of the outer loop exhibit the various perturbation directions. For example, at 05:13:59 UT in Figure 9a, the loop leg of P1 is shrinking, while the loop apex of P2 and another loop leg of P3 are expanding. At 05:15:35 UT in Figure 9b, the loop leg of P1 is expanding, while the loop apex of P2 and another loop leg of P3 are shrinking. Such anti-phase perturbations are possibly the signature of an MHD wave in the outer loop (see Duckenfield et al., 2019).

Figure 8. Time–distance images along three slits derived from the AIA 171 Å image series (**a**–**c**) and their running-difference (**d**–**f**). The white line profile in Panel **a** is the intensity curve at the site of ≈66″, as marked by the *red tick* on the left hand. The *overplotted blue and red* lines represent the rapidly varying components in NoRP 1 GHz and GOES 1−8 Å, respectively. The white arrows outline the velocity of jets. The *green curves* mark the loop perturbation.
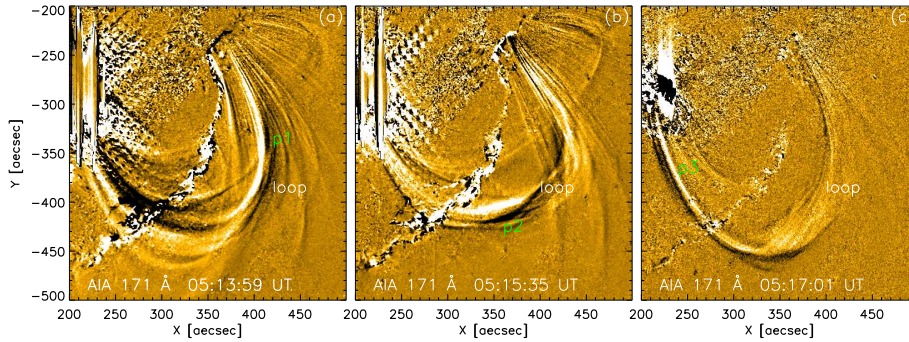
Figure 9. Running-difference images to show the outer loop in AIA 171 Å at 05:13:59 UT (**a**), 05:15:35 UT (**b**), 05:17:01 UT (**c**). P1−P3 mark the loop apex and two loop legs.

4. Conclusion and Discussion

Based on observations obtained by various instruments in X-rays, microwaves, and the UV, we investigate flare-related oscillations during the SOL2013-11-10T05:14 event. SDO/AIA in 1600 Å and 171 Å bands show that the X1.1 flare is a typical circular-ribbon flare. The spine–fan magnetic structure derived from the NLFFF extrapolation model (Wheatland, Sturrock, and Roumeliotis, 2000; Wiegelmann, 2004) confirmed the magnetic topology specific for the circular-ribbon flare. For instance, the dome-like structure is consistent with the closed circular ribbon: a set of overlying magnetic-field lines is consistent with the faint outer loop seen in the AIA 171 Å band image (see Figure 2). Our NLFFF extrapolation agrees with previous results using the potential magnetic-field extrapolation (e.g. Mészárosová et al., 2013). We found three types of oscillations, i.e. i) flare QPP with a quasi-period of roughly 20 seconds in the SXR/HXR, radio, and EUV channels, ii) periodic jets following the circular-ribbon flare with a cadence of about 72 seconds, iii) transverse perturbation with a duration of about 168 seconds at the faint outer loop.

The FFT and wavelet-analysis method are applied to determine the periodicity of the flare fluxes at multiple wavelengths, and they both show an oscillatory period of roughly 20 seconds. The wavelet spectra show an enhanced power over a broad range, but the wavelet power is always centered at the periodicity of around 20 seconds in SXR/HXR, radio, and EUV passbands. The GOES SXR flux shows a sharp increasing trend during the flare, so the small-amplitude QPPs only appear clearly during a short time interval, as shown in Figure 4c. They could be clearly seen during the whole flare time after normalization, as shown in Figure 4e. The flare QPP with a similar period can also be observed in the X-ray, radio/microwave, and EUV wavelengths recorded by other instruments. This is similar to previous observations (Nakariakov et al., 2010b; Milligan et al., 2017; Kupriyanova et al., 2020). The flare QPP with a broad period range of $10 - 83$ seconds has been found in a circular-ribbon flare (Mészárosová et al., 2013), which contains our 20-second periodicity. They further identified the wavelet tadpoles from the radio source and explained them as fast magnetoacoustic waves propagating in the coronal loop. However, we could not get the wavelet tadpoles from the wavelet power spectra. The flare QPP with a dominant period of ≈ 20 seconds is most likely to be triggered by the nonthermal process. Our multi-wavelength observations suggest the co-existence of thermal and nonthermal processes during the circular-ribbon flare. The flare QPP is detected in the SXR and EUV wavelengths, which is a thermal process. It is also seen in the microwave emissions, which are obviously decaying after reaching the maximum, indicating nonthermal gyrosynchrotron emission during the flare (Dulk, 1985; Warmuth et al., 2016; Li et al., 2020d). Moreover, the flare QPP can also be observed in the HXR and high-frequency (i.e. NoRP 35 GHz) microwave emissions, implying an energy-release process by nonthermal electrons. The Neupert effect (Neupert, 1968; Ning, 2008, 2009; Ning and Cao, 2010) is plasma heating as a result of energy released by nonthermal electrons. So, oscillations of the accelerated electron emission are a reason for oscillations detecting in thermal emissions in this study.

Similar to previous findings (e.g. Reid et al., 2012; Shen et al., 2012; Zhang et al., 2016; Lu et al., 2019), we found a series of coronal jets triggered by the circular-ribbon flare at the footpoint of the outer loop, and they appear a regular and repeated occurrence with an average periodicity of roughly 72 seconds. These periodic jets could be regarded as repeated outflows produced by the magnetic reconnection during the circular-ribbon flare (Chitta et al., 2017; Shen et al., 2019; Zhang, 2020). Therefore, the periodic jets at the footpoint might be produced by a nonthermal process during the circular-ribbon flare, i.e. the repetitive magnetic reconnection. This is consistent with previous findings (Kumar, Nakariakov, and Cho, 2015), who found that repeated magnetic reconnection at the footpoint could drive the periodic acceleration of nonthermal electrons. However, we could not detect the similar periodicity such as 72 seconds in flare light curves in HXR and microwave emissions, both of which are often related to the nonthermal electron. The dominant period of the flare QPP is about 20 seconds, which is far from the periodicity of coronal jets. So it is hard to conclude whether the flare QPP affected periodicity jets, or it was the result of them.

The outer loop appears to show a transverse perturbation with a duration of about 168 seconds in this event. The perturbation is similar to previous observations about the transverse oscillation in the outer loop of the circular-ribbon flare (e.g. Zhang et al., 2020; Dai et al., 2021). However, the perturbation feature studied here only persists for about a half cycle, and then disappears, so it can not be regarded as an oscillation or periodicity. Here, the 168 seconds are regarded as the perturbation duration of the loop apex and leg. It is interesting that loop apex perturbed within anti-phase to one of the loop legs, which would suggest that the loop perturbation is probably driven and modulated by a sausage wave (Tian et al., 2016; Li et al., 2020a) or a slow magnetoacoustic wave (Mészárosová et al., 2013; Kumar, Nakariakov, and Cho, 2015). It should be pointed out that the outer loop perturbation only remains a half cycle, which might be due to the large perturbation amplitude, since the decay time depends on the perturbation/oscillation amplitude (e.g., Goddard and Nakariakov, 2016).

Declarations

References

Amiri, S., Karami, K., Ebrahimi, Z.: 2021, Resonant absorption of kink MHD waves in inclined and asymmetric coronal loops. *Mon. Not. Roy. Astron. Soc.* **502**, 2172. DOI. ADS.

Anfinogentov, S.A., Nakariakov, V.M., Nisticò, G.: 2015, Decayless low-amplitude kink oscillations: a common phenomenon in the solar corona? *Astron. Astrophys.* **583**, A136. DOI. ADS.

Anfinogentov, S.A., Nakariakov, V.M., Pascoe, D.J., Goddard, C.R.: 2021, Solar Bayesian Analysis Toolkit—A New Markov Chain Monte Carlo IDL Code for Bayesian Parameter Inference. *Astrophys. J. Suppl.* **252**, 11. DOI. ADS.

Aptekar, R.L., Frederiks, D.D., Golenetskii, S.V., Ilynskii, V.N., Mazets, E.P., Panov, V.N., Sokolova, Z.J., Terekhov, M.M., Sheshin, L.O., Cline, T.L., Stilwell, D.E.: 1995, Konus-W Gamma-Ray Burst Experiment for the GGS Wind Spacecraft. *Space Sci. Rev.* **71**, 265. DOI. ADS.

Aschwanden, M.J.: 1987, Theory of Radio Pulsations in Coronal Loops. *Solar Phys.* **111**, 113. DOI. ADS.

Aschwanden, M.J., de Pontieu, B., Schrijver, C.J., Title, A.M.: 2002, Transverse Oscillations in Coronal Loops Observed with TRACE II. Measurements of Geometric and Physical Parameters. *Solar Phys.* **206**, 99. DOI. ADS.

Benz, A.O.: 2017, Flare Observations. *Liv. Rev. Solar Phys.* **14**, 2. DOI. ADS.

Brosius, J.W., Daw, A.N.: 2015, Quasi-periodic Fluctuations and Chromospheric Evaporation in a Solar Flare Ribbon Observed by IRIS. *Astrophys. J.* **810**, 45. DOI. ADS.

Cai, Q., Shen, C., Raymond, J.C., Mei, Z., Warmuth, A., Roussev, I.I., Lin, J.: 2019, Investigations of a supra-arcade fan and termination shock above the top of the flare-loop system of the 2017 September 10 event. *Mon. Not. Roy. Astron. Soc.* **489**, 3183. DOI. ADS.

Chen, P.F., Priest, E.R.: 2006, Transition-Region Explosive Events: Reconnection Modulated by p-Mode Waves. *Solar Phys.* **238**, 313. DOI. ADS.

Chen, X., Yan, Y., Tan, B., Huang, J., Wang, W., Chen, L., Zhang, Y., Tan, C., Liu, D., Masuda, S.: 2019, Quasi-periodic Pulsations before and during a Solar Flare in AR 12242. *Astrophys. J.* **878**, 78. DOI. ADS.

Chifor, C., Isobe, H., Mason, H.E., Hannah, I.G., Young, P.R., Del Zanna, G., Krucker, S., Ichimoto, K., Katsukawa, Y., Yokoyama, T.: 2008, Magnetic flux cancellation associated with a recurring solar jet observed with Hinode, RHESSI, and STEREO/EUVI. *Astron. Astrophys.* **491**, 279. DOI. ADS.

Chitta, L.P., Peter, H., Young, P.R., Huang, Y.-M.: 2017, Compact solar UV burst triggered in a magnetic field with a fan-spine topology. *Astron. Astrophys.* **605**, A49. DOI. ADS.

Clarke, B.P., Hayes, L.A., Gallagher, P.T., Maloney, S.A., Carley, E.P.: 2021, Quasi-periodic Particle Acceleration in a Solar Flare. *Astrophys. J.* **910**, 123. DOI. ADS.

Dai, J., Zhang, Q.M., Su, Y.N., Ji, H.S.: 2021, Transverse oscillation of a coronal loop induced by a flare-related jet. *Astron. Astrophys.* **646**, A12. DOI. ADS.

Didkovsky, L., Judge, D., Wieman, S., Woods, T., Jones, A.: 2012, EUV SpectroPhotometer (ESP) in Extreme Ultraviolet Variability Experiment (EVE): Algorithms and Calibrations. *Solar Phys.* **275**, 179. DOI. ADS.

Dolla, L., Marqué, C., Seaton, D.B., Van Doorsselaere, T., Dominique, M., Berghmans, D., Cabanas, C., De Groof, A., Schmutz, W., Verdini, A., West, M.J., Zender, J., Zhukov, A.N.: 2012, Time Delays in Quasi-periodic Pulsations Observed during the X2.2 Solar Flare on 2011 February 15. *Astrophys. J. Lett.* **749**, L16. DOI. ADS.

Dominique, M., Zhukov, A.N., Dolla, L., Inglis, A., Lapenta, G.: 2018, Detection of Quasi-Periodic Pulsations in Solar EUV Time Series. *Solar Phys.* **293**, 61. DOI. ADS.

Duckenfield, T.J., Goddard, C.R., Pascoe, D.J., Nakariakov, V.M.: 2019, Observational signatures of the third harmonic in a decaying kink oscillation of a coronal loop. *Astron. Astrophys.* **632**, A64. DOI. ADS.

Dulk, G.A.: 1985, Radio emission from the sun and stars. *Rev. Astron. Astrophys.* **23**, 169. DOI. ADS.

Feng, S., Yu, L., Wang, F., Deng, H., Yang, Y.: 2017, Midterm Periodicity Analysis of the Mount Wilson Magnetic Indices Using the Synchrosqueezing Transform. *Astrophys. J.* **845**, 11. DOI. ADS.

Feng, S., Deng, Z., Yuan, D., Xu, Z., Yang, X.: 2020, Propagating slow sausage waves in a sunspot observed by the New Vacuum Solar Telescope. *Res. Astron. Astrophys.* **20**, 117. DOI. ADS.

Fleishman, G.D., Fu, Q.J., Huang, G.-L., Melnikov, V.F., Wang, M.: 2002, Discovery of unusual large group delay in microwave millisecond oscillating events. *Astron. Astrophys.* **385**, 671. DOI. ADS.

Goddard, C.R., Nakariakov, V.M.: 2016, Dependence of kink oscillation damping on the amplitude. *Astron. Astrophys.* **590**, L5. DOI. ADS.

Goddard, C.R., Nisticò, G.: 2020, Temporal evolution of oscillating coronal loops. *Astron. Astrophys.* **638**, A89. DOI. ADS.

Guidoni, S.E., DeVore, C.R., Karpen, J.T., Lynch, B.J.: 2016, Magnetic-island Contraction and Particle Acceleration in Simulated Eruptive Solar Flares. *Astrophys. J.* **820**, 60. DOI. ADS.

Guo, Y., Cheng, X., Ding, M.: 2017, Origin and structures of solar eruptions II: Magnetic modeling. *Science China Earth Sciences* **60**, 1408. DOI. ADS.

Hanaoka, Y., Shibasaki, K., Nishio, M., Enome, S., Nakajima, H., Takano, T., Torii, C., Sekiguchi, H., Bushimata, T., Kawashima, S., Shinohara, N., Irimajiri, Y., Koshiishi, H., Kosugi, T., Shiomi, Y., Sawa, M., Kai, K.: 1994, Processing of the Nobeyama Radioheliograph Data. In: Enome, S., Hirayama, T. (eds.) *Proc. Kofu Symp.*, *Radioheliograph Series, 0911-05501, No. 6; NRO Report No. 36*, Nobeyama Radio Observatory, Nobeyama, 35. ADS.

Hao, Q., Yang, K., Cheng, X., Guo, Y., Fang, C., Ding, M.D., Chen, P.F., Li, Z.: 2017, A circular white-light flare with impulsive and gradual white-light kernels. *Nat. Comm.* **8**, 2202. DOI. ADS.

Hayes, L.A., Inglis, A.R., Christe, S., Dennis, B., Gallagher, P.T.: 2020, Statistical Study of GOES X-Ray Quasi-periodic Pulsations in Solar Flares. *Astrophys. J.* **895**, 50. DOI. ADS.

Hernandez-Perez, A., Thalmann, J.K., Veronig, A.M., Su, Y., Gömöry, P., Dickson, E.C.: 2017, Generation Mechanisms of Quasi-parallel and Quasi-circular Flare Ribbons in a Confined Flare. *Astrophys. J.* **847**, 124. DOI. ADS.

Inglis, A.R., Ireland, J., Dennis, B.R., Hayes, L., Gallagher, P.: 2016, A Large-scale Search for Evidence of Quasi-periodic Pulsations in Solar Flares. *Astrophys. J.* **833**, 284. DOI. ADS.

Karlický, M., Yasnov, L.V.: 2021, Spatial quasi-periodic variations of the plasma density and magnetic field in zebra radio sources. *Astron. Astrophys.* **646**, A179. DOI. ADS.

Kashapova, L.K., Kupriyanova, E.G., Xu, Z., Reid, H.A.S., Kolotkov, D.Y.: 2020, The origin of quasi-periodicities during circular ribbon flares. *Astron. Astrophys.* **642**, A195. DOI. ADS.

Kliem, B., Karlický, M., Benz, A.O.: 2000, Solar flare radio pulsations as a signature of dynamic magnetic reconnection. *Astron. Astrophys.* **360**, 715. ADS.

Kobanov, N.I., Chelpanov, A.A.: 2019, Oscillations Accompanying a He I 10830 Å Negative Flare in a Solar Facula II. Response of the Transition Region and Corona. *Solar Phys.* **294**, 58. DOI. ADS.

Kolotkov, D.Y., Nakariakov, V.M., Kupriyanova, E.G., Ratcliffe, H., Shibasaki, K.: 2015, Multi-mode quasi-periodic pulsations in a solar flare. *Astron. Astrophys.* **574**, A53. DOI. ADS.

Kolotkov, D.Y., Pugh, C.E., Broomhall, A.-M., Nakariakov, V.M.: 2018, Quasi-periodic Pulsations in the Most Powerful Solar Flare of Cycle 24. *Astrophys. J. Lett.* **858**, L3. DOI. ADS.

Kumar, P., Nakariakov, V.M., Cho, K.-S.: 2015, X-Ray and EUV Observations of Simultaneous Short and Long Period Oscillations in Hot Coronal Arcade Loops. *Astrophys. J.* **804**, 4. DOI. ADS.

Kupriyanova, E.G., Melnikov, V.F., Nakariakov, V.M., Shibasaki, K.: 2010, Types of Microwave Quasi-Periodic Pulsations in Single Flaring Loops. *Solar Phys.* **267**, 329. DOI. ADS.

Kupriyanova, E.G., Kashapova, L.K., Reid, H.A.S., Myagkova, I.N.: 2016, Relationship of Type III Radio Bursts with Quasi-periodic Pulsations in a Solar Flare. *Solar Phys.* **291**, 3427. DOI. ADS.

Kupriyanova, E., Kolotkov, D., Nakariakov, V., Kaufman, A.: 2020, Quasi-Periodic Pulsations in Solar and Stellar Flares. Review. *Solar-Terrestrial Physics* **6**, 3. DOI. ADS.

Leka, K.D., Barnes, G., Crouch, A.D., Metcalf, T.R., Gary, G.A., Jing, J., Liu, Y.: 2009, Resolving the 180° Ambiguity in Solar Vector Magnetic Field Data: Evaluating the Effects of Noise, Spatial Resolution, and Method Assumptions. *Solar Phys.* **260**, 83. DOI. ADS.

Lemen, J.R., Title, A.M., Akin, D.J., Boerner, P.F., Chou, C., Drake, J.F., Duncan, D.W., Edwards, C.G., Friedlaender, F.M., Heyman, G.F., Hurlburt, N.E., Katz, N.L., Kushner, G.D., Levay, M., Lindgren, R.W., Mathur, D.P., McFeaters, E.L., Mitchell, S., Rehse, R.A., Schrijver, C.J., Springer, L.A., Stern, R.A., Tarbell, T.D., Wuelser, J.-P., Wolfson, C.J., Yanari, C., Bookbinder, J.A., Cheimets, P.N., Caldwell, D., Deluca, E.E., Gates, R., Golub, L., Park, S., Podgorski, W.A., Bush, R.I., Scherrer, P.H., Gummin, M.A., Smith, P., Auker, G., Jerram, P., Pool, P., Soufli, R., Windt, D.L., Beardsley, S., Clapp, M., Lang, J., Waltham, N.: 2012, The Atmospheric Imaging Assembly (AIA) on the Solar Dynamics Observatory (SDO). *Solar Phys.* **275**, 17. DOI. ADS.

Li, B., Antolin, P., Guo, M.-Z., Kuznetsov, A.A., Pascoe, D.J., Van Doorsselaere, T., Vasheghani Farahani, S.: 2020a, Magnetohydrodynamic Fast Sausage Waves in the Solar Corona. *Space Sci. Rev.* **216**, 136. DOI. ADS.

Li, D.: 2021, TBD. *Sci. China Tech. Sci.*, 64. DOI.

Li, D., Zhang, Q.M.: 2017, Quasi-periodic pulsations with multiple periods in hard X-ray emission. *Mon. Not. Roy. Astron. Soc.* **471**, L6. DOI. ADS.

Li, D., Ning, Z.J., Zhang, Q.M.: 2015, Imaging and Spectral Observations of Quasi-periodic Pulsations in a Solar Flare. *Astrophys. J.* **807**, 72. DOI. ADS.

Li, D., Yuan, D., Su, Y.N., Zhang, Q.M., Su, W., Ning, Z.J.: 2018a, Non-damping oscillations at flaring loops. *Astron. Astrophys.* **617**, A86. DOI. ADS.

Li, D., Feng, S., Su, W., Huang, Y.: 2020b, Preflare very long-periodic pulsations observed in Hα emission before the onset of a solar flare. *Astron. Astrophys.* **639**, L5. DOI. ADS.

Li, D., Lu, L., Ning, Z., Feng, L., Gan, W., Li, H.: 2020c, Quasi-periodic Pulsation Detected in Lyα Emission During Solar Flares. *Astrophys. J.* **893**, 7. DOI. ADS.

Li, D., Kolotkov, D.Y., Nakariakov, V.M., Lu, L., Ning, Z.J.: 2020d, Quasi-periodic Pulsations of Gamma-Ray Emissions from a Solar Flare on 2017 September 6. *Astrophys. J.* **888**, 53. DOI. ADS.

Li, D., Warmuth, A., Lu, L., Ning, Z.: 2021a, An investigation of flare emissions at multiple wavelengths. *Research in Astronomy and Astrophysics* **21**, 066. DOI. ADS.

Li, D., Ge, M., Dominique, M., Zhao, H., Li, G., Li, X., Zhang, S., Lu, F., Gan, W., Ning, Z.: 2021b, Detection of Flare Multiperiodic Pulsations in Mid-ultraviolet Balmer Continuum, Lyα, Hard X-Ray, and Radio Emissions Simultaneously. *Astrophys. J.* **921**, 179. DOI. ADS.

Li, T., Zhang, J.: 2015, Quasi-periodic Slipping Magnetic Reconnection During an X-class Solar Flare Observed by the Solar Dynamics Observatory and Interface Region Imaging Spectrograph. *Astrophys. J. Lett.* **804**, L8. DOI. ADS.

Li, T., Yang, S., Zhang, Q., Hou, Y., Zhang, J.: 2018b, Two Episodes of Magnetic Reconnections during a Confined Circular-ribbon Flare. *Astrophys. J.* **859**, 122. DOI. ADS.

Liang, B., Meng, Y., Feng, S., Yang, Y.: 2020, Estimating red noise in quasi-periodic signals with MCMC-based Bayesian. *Astrophys. Space Sci.* **365**, 40. DOI. ADS.

Lim, D., Nakariakov, V.M., Moon, Y.-J.: 2018, Sausage oscillations in a plasma cylinder with a surface current. *J. Atmos. Solar-Terr. Phys.* **175**, 49. DOI. ADS.

Lin, R.P., Dennis, B.R., Hurford, G.J., Smith, D.M., Zehnder, A., Harvey, P.R., Curtis, D.W., Pankow, D., Turin, P., Bester, M., Csillaghy, A., Lewis, M., Madden, N., van Beek, H.F., Appleby, M., Raudorf, T., McTiernan, J., Ramaty, R., Schmahl, E., Schwartz, R., Krucker, S., Abiad, R., Quinn, T., Berg, P., Hashii, M., Sterling, R., Jackson, R., Pratt, R., Campbell, R.D., Malone, D., Landis, D., Barrington-Leigh, C.P., Slassi-Sennou, S., Cork, C., Clark, D., Amato, D., Orwig, L., Boyle, R., Banks, I.S., Shirey, K., Tolbert, A.K., Zarro, D., Snow, F., Thomsen, K., Henneck, R., McHedlishvili, A., Ming, P., Fivian, M., Jordan, J., Wanner, R., Crubb, J., Preble, J., Matranga, M., Benz, A., Hudson, H., Canfield, R.C., Holman, G.D., Crannell, C., Kosugi, T., Emslie, A.G., Vilmer, N., Brown, J.C., Johns-Krull, C., Aschwanden, M., Metcalf, T., Conway, A.: 2002, The Reuven Ramaty High-Energy Solar Spectroscopic Imager (RHESSI). *Solar Phys.* **210**, 3. DOI. ADS.

Liu, W., Berger, T.E., Title, A.M., Tarbell, T.D., Low, B.C.: 2011, Chromospheric Jet and Growing "Loop" Observed by Hinode: New Evidence of Fan-spine Magnetic Topology Resulting from Flux Emergence. *Astrophys. J.* **728**, 103. DOI. ADS.

Lu, L., Feng, L., Li, Y., Li, D., Ning, Z., Gan, W.: 2019, Spectroscopic and Stereoscopic Observations of the Solar Jets. *Astrophys. J.* **887**, 154. DOI. ADS.

Lu, L., Li, D., Ning, Z., Feng, L., Gan, W.: 2021, Quasi-Periodic Pulsations Detected in Ly α and Nonthermal Emissions During Solar Flares. *Solar Phys.* **296**, 130. DOI. ADS.

Masson, S., Pariat, E., Aulanier, G., Schrijver, C.J.: 2009, The Nature of Flare Ribbons in Coronal Null-Point Topology. *Astrophys. J.* **700**, 559. DOI. ADS.

McLaughlin, J.A., Nakariakov, V.M., Dominique, M., Jelínek, P., Takasao, S.: 2018, Modelling Quasi-Periodic Pulsations in Solar and Stellar Flares. *Space Sci. Rev.* **214**, 45. DOI. ADS.

Meegan, C., Lichti, G., Bhat, P.N., Bissaldi, E., Briggs, M.S., Connaughton, V., Diehl, R., Fishman, G., Greiner, J., Hoover, A.S., van der Horst, A.J., von Kienlin, A., Kippen, R.M., Kouveliotou, C., McBreen, S., Paciesas, W.S., Preece, R., Steinle, H., Wallace, M.S., Wilson, R.B., Wilson-Hodge, C.: 2009, The Fermi Gamma-ray Burst Monitor. *Astrophys. J.* **702**, 791. DOI. ADS.

Mészárosová, H., Dudík, J., Karlický, M., Madsen, F.R.H., Sawant, H.S.: 2013, Fast Magnetoacoustic Waves in a Fan Structure Above a Coronal Magnetic Null Point. *Solar Phys.* **283**, 473. DOI. ADS.

Metcalf, T.R., Leka, K.D., Barnes, G., Lites, B.W., Georgoulis, M.K., Pevtsov, A.A., Balasubramaniam, K.S., Gary, G.A., Jing, J., Li, J., Liu, Y., Wang, H.N., Abramenko, V., Yurchyshyn, V., Moon, Y.-J.: 2006, An Overview of Existing Algorithms for Resolving the 180° Ambiguity in Vector Magnetic Fields: Quantitative Tests with Synthetic Data. *Solar Phys.* **237**, 267. DOI. ADS.

Milligan, R.O., Fleck, B., Ireland, J., Fletcher, L., Dennis, B.R.: 2017, Detection of Three-minute Oscillations in Full-disk Lyα Emission during a Solar Flare. *Astrophys. J. Lett.* **848**, L8. DOI. ADS.

Nakajima, H., Sekiguchi, H., Sawa, M., Kai, K., Kawashima, S.: 1985, The radiometer and polarimeters at 80, 35, and 17 GHz for solar observations at Nobeyama. *Pub. Astron. Soc. Japan* **37**, 163. ADS.

Nakariakov, V.M., Kolotkov, D.Y.: 2020, Magnetohydrodynamic Waves in the Solar Corona. *Rev. Astron. Astrophys.* **58**, 441. DOI. ADS.

Nakariakov, V.M., Zimovets, I.V.: 2011, Slow Magnetoacoustic Waves in Two-ribbon Flares. *Astrophys. J. Lett.* **730**, L27. DOI. ADS.

Nakariakov, V.M., Ofman, L., Deluca, E.E., Roberts, B., Davila, J.M.: 1999, TRACE observation of damped coronal loop oscillations: Implications for coronal heating. *Science* **285**, 862. DOI. ADS.

Nakariakov, V.M., Inglis, A.R., Zimovets, I.V., Foullon, C., Verwichte, E., Sych, R., Myagkova, I.N.: 2010a, Oscillatory processes in solar flares. *Plasma Phys. Control. Fusion* **52**, 124009. DOI. ADS.

Nakariakov, V.M., Foullon, C., Myagkova, I.N., Inglis, A.R.: 2010b, Quasi-Periodic Pulsations in the Gamma-Ray Emission of a Solar Flare. *Astrophys. J. Lett.* **708**, L47. DOI. ADS.

Nakariakov, V.M., Anfinogentov, S., Storozhenko, A.A., Kurochkin, E.A., Bogod, V.M., Sharykin, I.N., Kaltman, T.I.: 2018, Quasi-periodic Pulsations in a Solar Microflare. *Astrophys. J.* **859**, 154. DOI. ADS.

Nakariakov, V.M., Anfinogentov, S.A., Antolin, P., Jain, R., Kolotkov, D.Y., Kupriyanova, E.G., Li, D., Magyar, N., Nisticò, G., Pascoe, D.J., Srivastava, A.K., Terradas, J., Vasheghani Farahani, S., Verth, G., Yuan, D., Zimovets, I.V.: 2021, Kink Oscillations of Coronal Loops. *Space Sci. Rev.* **217**, 73. DOI. ADS.

Neupert, W.M.: 1968, Comparison of Solar X-Ray Line Emission with Microwave Emission during Flares. *Astrophys. J. Lett.* **153**, L59. DOI. ADS.

Ning, Z.: 2008, RHESSI Observations of the Neupert Effect in Three Solar Flares. *Solar Phys.* **248**, 99. DOI. ADS.

Ning, Z.: 2009, The investigation of the Neupert effect in two solar flares. *Science in China: Physics, Mechanics and Astronomy* **52**, 1686. DOI. ADS.

Ning, Z.: 2014, Imaging Observations of X-Ray Quasi-periodic Oscillations at 3 - 6 keV in the 26 December 2002 Solar Flare. *Solar Phys.* **289**, 1239. DOI. ADS.

Ning, Z.: 2017, One-Minute Quasi-Periodic Pulsations Seen in a Solar Flare. *Solar Phys.* **292**, 11. DOI. ADS.

Ning, Z., Cao, W.: 2010, Investigation of the Neupert Effect in the Various Intervals of Solar Flares. *Solar Phys.* **264**, 329. DOI. ADS.

Ning, Z., Ding, M.D., Wu, H.A., Xu, F.Y., Meng, X.: 2005, Microwave type III bursts and pulsation groups. *Astron. Astrophys.* **437**, 691. DOI. ADS.

Ofman, L., Wang, T.: 2002, Hot Coronal Loop Oscillations Observed by SUMER: Slow Magnetosonic Wave Damping by Thermal Conduction. *Astrophys. J. Lett.* **580**, L85. DOI. ADS.

Pal'shin, V.D., Charikov, Y.E., Aptekar, R.L., Golenetskii, S.V., Kokomov, A.A., Svinkin, D.S., Sokolova, Z.Y., Ulanov, M.V., Frederiks, D.D., Tsvetkova, A.E.: 2014, Konus- Wind and Helicon- Coronas-F observations of solar flares. *Geomag. Aeron.* **54**, 943. DOI. ADS.

Parks, G.K., Winckler, J.R.: 1969, Sixteen-Second Periodic Pulsations Observed in the Correlated Microwave and Energetic X-Ray Emission from a Solar Flare. *Astrophys. J. Lett.* **155**, L117. DOI. ADS.

Pesnell, W.D., Thompson, B.J., Chamberlin, P.C.: 2012, The Solar Dynamics Observatory (SDO). *Solar Phys.* **275**, 3. DOI. ADS.

Priest, E.R., Forbes, T.G.: 2002, The magnetic nature of solar flares. *Astron. Astrophys. Rev.* **10**, 313. DOI. ADS.

Pugh, C.E., Nakariakov, V.M., Broomhall, A.-M., Bogomolov, A.V., Myagkova, I.N.: 2017, Properties of quasi-periodic pulsations in solar flares from a single active region. *Astron. Astrophys.* **608**, A101. DOI. ADS.

Reid, H.A.S., Vilmer, N., Aulanier, G., Pariat, E.: 2012, X-ray and ultraviolet investigation into the magnetic connectivity of a solar flare. *Astron. Astrophys.* **547**, A52. DOI. ADS.

Samanta, T., Tian, H., Chen, B., Reeves, K.K., Cheung, M.C.M., Vourlidas, A., Banerjee, D.: 2021, Plasma heating induced by tadpole-like downflows in the flaring solar corona. *The Innovation* **2**, 100083. DOI. ADS.

Schou, J., Scherrer, P.H., Bush, R.I., Wachter, R., Couvidat, S., Rabello-Soares, M.C., Bogart, R.S., Hoeksema, J.T., Liu, Y., Duvall, T.L., Akin, D.J., Allard, B.A., Miles, J.W., Rairden, R., Shine, R.A., Tarbell, T.D., Title, A.M., Wolfson, C.J., Elmore, D.F., Norton, A.A., Tomczyk, S.: 2012, Design and Ground Calibration of the Helioseismic and Magnetic Imager (HMI) Instrument on the Solar Dynamics Observatory (SDO). *Solar Phys.* **275**, 229. DOI. ADS.

Shen, Y., Liu, Y., Su, J., Deng, Y.: 2012, On a Coronal Blowout Jet: The First Observation of a Simultaneously Produced Bubble-like CME and a Jet-like CME in a Solar Event. *Astrophys. J.* **745**, 164. DOI. ADS.

Shen, Y., Liu, Y., Song, T., Tian, Z.: 2018, A Quasi-periodic Fast-propagating Magnetosonic Wave Associated with the Eruption of a Magnetic Flux Rope. *Astrophys. J.* **853**, 1. DOI. ADS.

Shen, Y., Qu, Z., Zhou, C., Duan, Y., Tang, Z., Yuan, D.: 2019, Round-trip Slipping Motion of the Circular Flare Ribbon Evidenced in a Fan-spine Jet. *Astrophys. J. Lett.* **885**, L11. DOI. ADS.

Shibata, K., Magara, T.: 2011, Solar Flares: Magnetohydrodynamic Processes. *Liv. Rev. Solar Phys.* **8**, 6. DOI. ADS.

Simões, P.J.A., Hudson, H.S., Fletcher, L.: 2015, Soft X-Ray Pulsations in Solar Flares. *Solar Phys.* **290**, 3625. DOI. ADS.

Song, Y., Tian, H.: 2018, Investigation of White-light Emission in Circular-ribbon Flares. *Astrophys. J.* **867**, 159. DOI. ADS.

Srivastava, A.K., Zaqarashvili, T.V., Uddin, W., Dwivedi, B.N., Kumar, P.: 2008, Observation of multiple sausage oscillations in cool post-flare loop. *Mon. Not. Roy. Astron. Soc.* **388**, 1899. DOI. ADS.

Sturrock, P.A., Coppi, B.: 1964, A New Model of Solar Flares. *Nature* **204**, 61. DOI. ADS.

Su, W., Guo, Y., Erdélyi, R., Ning, Z.J., Ding, M.D., Cheng, X., Tan, B.L.: 2018, Period Increase and Amplitude Distribution of Kink Oscillation of Coronal Loop. *Sci. Rep.* **8**, 4471. DOI. ADS.

Takasao, S., Shibata, K.: 2016, Above-the-loop-top Oscillation and Quasi-periodic Coronal Wave Generation in Solar Flares. *Astrophys. J.* **823**, 150. DOI. ADS.

Tan, B., Zhang, Y., Tan, C., Liu, Y.: 2010, Microwave Quasi-Periodic Pulsations in Multi-timescales Associated with a Solar Flare/CME Event. *Astrophys. J.* **723**, 25. DOI. ADS.

Tan, B., Yu, Z., Huang, J., Tan, C., Zhang, Y.: 2016, Very Long-period Pulsations before the Onset of Solar Flares. *Astrophys. J.* **833**, 206. DOI. ADS.

Tian, H., Young, P.R., Reeves, K.K., Wang, T., Antolin, P., Chen, B., He, J.: 2016, Global Sausage Oscillation of Solar Flare Loops Detected by the Interface Region Imaging Spectrograph. *Astrophys. J. Lett.* **823**, L16. DOI. ADS.

Török, T., Aulanier, G., Schmieder, B., Reeves, K.K., Golub, L.: 2009, Fan-Spine Topology Formation Through Two-Step Reconnection Driven by Twisted Flux Emergence. *Astrophys. J.* **704**, 485. DOI. ADS.

Torrence, C., Compo, G.P.: 1998, A Practical Guide to Wavelet Analysis. *Bull. Am. Metor. Soc.* **79**, 61. DOI. ADS.

Van Doorsselaere, T., Kupriyanova, E.G., Yuan, D.: 2016, Quasi-periodic Pulsations in Solar and Stellar Flares: An Overview of Recent Results (Invited Review). *Solar Phys.* **291**, 3143. DOI. ADS.

Vaughan, S.: 2005, A simple test for periodic signals in red noise. *Astron. Astrophys.* **431**, 391. DOI. ADS.

Wang, H., Liu, C.: 2012, Circular Ribbon Flares and Homologous Jets. *Astrophys. J.* **760**, 101. DOI. ADS.

Wang, T., Solanki, S.K., Curdt, W., Innes, D.E., Dammasch, I.E.: 2002, Doppler Shift Oscillations of Hot Solar Coronal Plasma Seen by SUMER: A Signature of Loop Oscillations? *Astrophys. J. Lett.* **574**, L101. DOI. ADS.

Wang, T., Ofman, L., Yuan, D., Reale, F., Kolotkov, D.Y., Srivastava, A.K.: 2021, Slow-Mode Magnetoacoustic Waves in Coronal Loops. *Space Sci. Rev.* **217**, 34. DOI. ADS.

Wang, Z.-K., Feng, S., Deng, L.-H., Meng, Y.: 2020, Spatial distributions of sunspot oscillation modes at different temperatures. *Research in Astronomy and Astrophysics* **20**, 006. DOI. ADS.

Warmuth, A., Shibasaki, K., Iwai, K., Mann, G.: 2016, Microwave observations of a large-scale coronal wave with the Nobeyama radioheliograph. *Astron. Astrophys.* **593**, A102. DOI. ADS.

Wheatland, M.S., Sturrock, P.A., Roumeliotis, G.: 2000, An Optimization Approach to Reconstructing Force-free Fields. *Astrophys. J.* **540**, 1150. DOI. ADS.

Wiegelmann, T.: 2004, Optimization code with weighting function for the reconstruction of coronal magnetic fields. *Solar Phys.* **219**, 87. DOI. ADS.

Woods, T.N., Eparvier, F.G., Hock, R., Jones, A.R., Woodraska, D., Judge, D., Didkovsky, L., Lean, J., Mariska, J., Warren, H., McMullin, D., Chamberlin, P., Berthiaume, G., Bailey, S., Fuller-Rowell, T., Sojka, J., Tobiska, W.K., Viereck, R.: 2012, Extreme Ultraviolet Variability Experiment (EVE) on the Solar Dynamics Observatory (SDO): Overview of Science Objectives, Instrument Design, Data Products, and Model Developments. *Solar Phys.* **275**, 115. DOI. ADS.

Xue, J., Su, Y., Li, H., Zhao, X.: 2020, Thermodynamical Evolution of Supra-arcade Downflows. *Astrophys. J.* **898**, 88. DOI. ADS.

Yan, X.L., Yang, L.H., Xue, Z.K., Mei, Z.X., Kong, D.F., Wang, J.C., Li, Q.L.: 2018, Simultaneous Observation of a Flux Rope Eruption and Magnetic Reconnection during an X-class Solar Flare. *Astrophys. J. Lett.* **853**, L18. DOI. ADS.

Yang, S., Xiang, Y.: 2016, Oscillation of Newly Formed Loops after Magnetic Reconnection in the Solar Chromosphere. *Astrophys. J. Lett.* **819**, L24. DOI. ADS.

Yu, S., Chen, B.: 2019, Possible Detection of Subsecond-period Propagating Magnetohydrodynamics Waves in Post-reconnection Magnetic Loops during a Two-ribbon Solar Flare. *Astrophys. J.* **872**, 71. DOI. ADS.

Yuan, D., Van Doorsselaere, T.: 2016, Forward Modeling of Standing Kink Modes in Coronal Loops. I. Synthetic Views. *Astrophys. J. Suppl.* **223**, 23. DOI. ADS.

Yuan, D., Feng, S., Li, D., Ning, Z., Tan, B.: 2019, A Compact Source for Quasi-periodic Pulsation in an M-class Solar Flare. *Astrophys. J. Lett.* **886**, L25. DOI. ADS.

Zhang, Q.M.: 2020, Simultaneous transverse oscillations of a coronal loop and a filament excited by a circular-ribbon flare. *Astron. Astrophys.* **642**, A159. DOI. ADS.

Zhang, Q.M., Li, D., Ning, Z.J., Su, Y.N., Ji, H.S., Guo, Y.: 2016, Explosive Chromospheric Evaporation in a Circular-ribbon Flare. *Astrophys. J.* **827**, 27. DOI. ADS.

Zhang, Q.M., Dai, J., Xu, Z., Li, D., Lu, L., Tam, K.V., Xu, A.A.: 2020, Transverse coronal loop oscillations excited by homologous circular-ribbon flares. *Astron. Astrophys.* **638**, A32. DOI. ADS.

Zhang, Q.M., Huang, Z.H., Hou, Y.J., Li, D., Ning, Z.J., Wu, Z.: 2021, Spectroscopic observations of a flare-related coronal jet. *Astron. Astrophys.* **647**, A113. DOI. ADS.

Zimovets, I.V., McLaughlin, J.A., Srivastava, A.K., Kolotkov, D.Y., Kuznetsov, A.A., Kupriyanova, E.G., Cho, I.-H., Inglis, A.R., Reale, F., Pascoe, D.J., Tian, H., Yuan, D., Li, D., Zhang, Q.M.: 2021, Quasi-Periodic Pulsations in Solar and Stellar Flares: A Review of Underpinning Physical Mechanisms and Their Predicted Observational Signatures. *Space Sci. Rev.* **217**, 66. DOI. ADS.